Inhibitory mechanisms and interaction of tangeretin, 5-demethyltangeretin, nobiletin, and 5-demethylnobiletin from citrus peels on pancreatic lipase: Kinetics, spectroscopies, and molecular dynamics simulation

Xin Huang, Junxiang Zhu, Li Wang, Huijuan Jing, Chaoyang Ma, Xingran Kou, Hongxin Wang

PII: S0141-8130(20)34064-2

DOI: https://doi.org/10.1016/j.ijbiomac.2020.07.305

Reference: BIOMAC 16353

To appear in: *International Journal of Biological Macromolecules*

Received date: 25 April 2020

Revised date: 11 July 2020

Accepted date: 29 July 2020

Please cite this article as: X. Huang, J. Zhu, L. Wang, et al., Inhibitory mechanisms and interaction of tangeretin, 5-demethyltangeretin, nobiletin, and 5-demethylnobiletin from citrus peels on pancreatic lipase: Kinetics, spectroscopies, and molecular dynamics simulation, *International Journal of Biological Macromolecules* (2020), https://doi.org/10.1016/j.ijbiomac.2020.07.305

Inhibitory mechanisms and interaction of tangeretin, 5-demethyltangeretin, nobiletin, and 5-demethylnobiletin from citrus peels on pancreatic lipase: Kinetics, spectroscopies, and molecular dynamics simulation

Xin Huang[a, b], Junxiang Zhu[c], Li Wang[a, b], Huijuan Jing[a, b], Chaoyang Ma[a, b], Xingran Kou[d*], Hongxin Wang[a, b*]

[a] School of Food Science and Technology, Jiangnan University, Wuxi, Jiangsu, 214122, People's Republic of China.

[b] State Key Laboratory of Food Science and Technology, Jiangnan University, Wuxi, Jiangsu, 214122, People's Republic of China.

[c] College of Food Science and Engineering, Qingdao Agricultural University, Qingdao 266109, People's Republic of China.

[d] School of Perfume and Aroma Technology, Shanghai Institute of Technology, Shanghai 201418, People's Republic of China.

*Co-corresponding author: Tel: (086)510-85917795; Fax: (086)510-85329276; E-mail: hxwang@jiangnan.edu.cn (H. Wang); kxran@163.com (X. Kou)

Abstract

This study aimed to reveal the interaction and inhibitory mechanisms of tangeretin (TAN), nobiletin (NBT), and their acidic hydroxylated forms, 5-demethyltangeretin (5-DT) and 5-demethylnobiletin (5-DN) on porcine pancreatic lipase (PPL) using spectroscopic techniques and molecular dynamics (MD) simulation. PPL inhibition assay showed that the inhibitory activity of NBT (IC_{50} value of 3.60±0.19 μM) was superior to those of three polymethoxylated flavones (PMFs), indicating it may be related to the methoxy groups at the 3′-position in its molecular structure. Inhibition kinetic analyses demonstrated that the inhibition types of the 4 PMFs were consistent with the mixed inhibition model, which agreed well with the results from the ultraviolet-visible (UV-Vis) spectroscopy, Circular dichroism (CD), fluorescence spectroscopy, molecular docking, and MD simulation that PMFs could bind to the PPL catalytic site and non-catalytic site, affecting the normal spatial conformation of PPL and weakening its ability to decompose the substrate. All these findings suggest that PMFs are a kind of natural lipase inhibitors, and NBT has the potential as a lipase inhibition precursor because of its unique flavone skeleton structure.

Keywords

Lipase inhibition; Polymethoxylated flavones; Inhibition mechanism; Molecular dynamics.

1. Introduction

Obesity is a chronic metabolic disease resulting from excessive calorie intake and fat metabolism disorders [1]. Obesity can induce a series of metabolic diseases, such as hypertension, type 2 diabetes, fatty liver disease, obstructive sleep apnea, cardiovascular diseases, and even certain cancers [2-4]. Currently, obesity has replaced undernutrition as the gravest threat to public health and survival in the 21st century [5]. The Lancet Commission reported that obesity affects more than two billion people worldwide, and by 2025, nearly 124 million children and adolescents are predicted to be obese [5]. Therefore, it is crucial to search for solutions for obesity on a global scale. An important strategy for the treatment of obesity includes the development of inhibitors of nutrient digestion and absorption [6]. Lipase (EC 3.1.1.3) is a key enzyme responsible for breaking down dietary triacylglycerol into absorbable monoglycerides and fatty acids [7]. Increasing evidence has demonstrated that inhibition of lipase to reduce lipid adsorption is a potential approach to alleviate obesity [8]. At present, the only clinically approved pancreatic lipase inhibitor is Orlistat [9]. However, gastrointestinal side effects, such as flatulence and diarrhea, may reduce patient compliance and limit its use [10]. Therefore, it is necessary to search for effective and safe lipase inhibitors as alternatives for clinical use.

A number of studies have focused on natural plant materials, including polyphenols, flavonoids, carotenoids, and polysaccharides, which exhibit weight loss and lipid-lowering bioactivities with low toxicity and side effects *in vitro* and *in vivo* [11-14]. Polymethoxylated flavones (PMFs) are a unique series of substances

belonging to the flavonoids family that are present in citrus fruit peels [15]. TAN and NBT are the most abundant compounds in citrus peels, and they have been found to possess physiological properties of anti-inflammation [16], anti-oxidation [17], and improving diabetes and lipid metabolism [18, 19]. Many studies have shown that PMFs can reduce fat and significantly prevent obesity by lowering cholesterol [20], inhibiting stearoyl-CoA desaturase mRNA expression [21], regulating lipid metabolism [22], and lowering blood glucose [23] *in vivo*. However, in recent years, some studies have suggested that direct interaction of PMFs with lipase may be another possible mechanism of their lipid-lowering activity. Zeng et al. investigated the anti-lipase activity of the Citri reticulatae pericarpium in different harvest periods and inferred that NBT might most likely act as the lipase inhibitor [24]. Our previous study also demonstrated that TAN and 5-demethyltangeretin (5-DT) had good antioxidant and lipase inhibitory effects *in vitro* [25], but their interaction and inhibition mechanisms remain unclear. A recent study has reported the existence of 78 PMFs in citrus, and their bioactivity may be greatly influenced by the number and position of methoxy groups [26]. Kawaguchi, Mizuno, Aida and Uchino [27] found that the hydroxyl group and the methoxy group at the 3′ and 4′ position of the flavonoid skeleton B ring of hesperidin could play an important role in the inhibitory activity (IC_{50}=32 μg/mL) of pancreatic lipase. However, the relationship between structure of PMFs and their lipase inhibitory activity remains largely unknown.

To understand the relationship between the structural characteristics of PMFs and their inhibition of lipase activity, we have isolated and purified TAN and NBT from

citrus peels and obtained their corresponding hydroxylated products at 5-position, including 5-DT and 5-demethylnobiletin (5-DN), by acid hydrolysis. Interestingly, according to the order of compounds 5-DT (2), TAN (1) and 5-DN (4), and NBT (3) (Fig. 1), the structure of the latter compound has one more methoxy group at 5 or 3′ positions than the former compound. In this study, the inhibition rates and mechanisms of these PMFs on lipase were examined by lipase inhibition kinetic experiments. Meanwhile, multispectral analysis and molecular dynamics (MD) simulation techniques such as UV-visible analysis, CD spectrum, and fluorescence spectroscopy were also conducted to confirm the interaction and mechanisms between PMFs and lipase. Therefore, this study aims to analyze the key functional groups of PMFs inhibiting lipase and reveal the molecular mechanism of their lipase inhibitory activity.

2. Materials and methods

2.1 Chemicals and Materials

Porcine pancreatic lipase (PPL, type II), 4-methylumbelliferyl (4-MU) oleate, and dimethyl sulfoxide (DMSO) were purchased from Sigma-Aldrich (St Louis, MO, USA). Ethyl acetate, n-hexane, ethanol, phosphoric acid, citric acid, disodium hydrogen phosphate, sodium dihydrogen phosphate, and 200–300 mesh (50–75 μm) column separation of silica gel were all purchased from Sinopharm Chemical Reagent Co., Ltd (Shanghai, China). Double-distilled water was used. Chromatographic grade methanol, acetonitrile, and formic acid were purchased from Merck (Darmstadt, Germany). The tangeretin and nobiletin, used as standards (purity of 95%), were

purchased from Shanghai Aladdin Biotechnology Co., Ltd (Shanghai, China).

2.2 Conversion of TAN and NBT to 5-DT and 5-DN

5-DT and 5-DN were obtained by acid hydrolysis of TAN and NBT. The specific method for converting TAN and NBT to 5-DT and 5-DN with acid hydrolysis has been reported in our previous study [25]. The transformed products were further purified by a silica gel column and eluted with n-hexane/ethyl acetate (1:1, v/v). The eluent was monitored by HPLC and evaporated to dryness under vacuum. The isolated products were identified using ultra-high performance liquid chromatography coupled with mass spectrometry (UPLC-TOF-MS). The detailed method of UPLC-TOF-MS was listed in Supplementary Materials.

2.3 Real time-inhibition of PPL

The inhibitory activity of PMFs against PPL, (Sigma type II) was monitored in real-time according to the procedure described previously[28]. In the assay, 4-methylumbelliferone (4-MU) oleate was used as the substrate, which is hydrolyzed by PPL to 4-MU, a fluorescent product that can be monitored at the excitation and emission wavelength of 340 nm and 460 nm, respectively. A 50 μL PPL solution (0.01 mg/mL, final concentration) and 50 μL different concentrations inhibitors (1, 5, 10, 15, 25, 50, 100, and 200 μM) dissolved in 0.1 M citrate phosphate buffer (0.1 M citrate-Na_2HPO_4, pH 8.0) were mixed and incubated at 37 ℃ for 10 min in a 96-well plate. Then, 100 μL 4-MU oleate (10 μM, final concentration) was added to initiate the reaction, with the final concentration of DMSO at 1% (v/v, without loss of the

catalytic activity). The fluorescence signals of each well were measured every 60 s using a microplate reader (SynergyTM2, BioTek Instruments Inc., Winooski, VT, USA) within 35 min of incubation at 37 ℃. Citrate phosphate buffer with sample (no PPL added) was used as the sample control group, citrate phosphate buffer with PPL (no sample added) as the blank group, and citrate phosphate buffer only as the blank control group. The PPL inhibitory rate (1) was calculated as follows:

$$\text{Inhibition rate (\%)} = [1-(A1-A2)/(A3-A4)] \times 100\% \quad (1)$$

where A1, A2, A3, and A4 were defined as fluorescence signals of the sample group, the sample control group, the blank group, and the blank control group, respectively.

2.4 Inhibitory kinetic analysis

The inhibitory kinetics of TAN (1), 5-DT (2), NBT (3), and 5-DN (4) against PPL were studied by the Lineweaver-Burk equation. Initial velocity (v) for various substrate concentrations against different inhibitor concentrations was determined [28]. The inhibition type of the PMFs was analyzed based on the Lineweaver-Burk plot, and the corresponding inhibition constant (K_i) was calculated by GraphPad Prism 7.5 software (San Diego, Canada). The following equations for competitive inhibition Eq. (2), noncompetitive inhibition Eq. (3), or mixed inhibition Eq. (4) were used to calculate the K_i values.

$$V = (V_{\max} S) / \left[K_{\mathrm{m}} (+I / K_i) + S\right] \quad (2)$$

$$V = (V_{\max} S) / \left[(K_{\mathrm{m}} + S)(1 + I / K_i)\right] \quad (3)$$

$$V = (V_{\max} S) / [(1+I / K_i) K_m+(1+I / \alpha K_i) S] \quad (4)$$

where V and V_{max} are the enzymatic reaction velocity and maximum velocity, respectively; S and I represent the substrate and inhibitor concentrations, respectively; and K_i and K_m is the inhibition constant and the Michaelis constant (substrate concentration at 0.5 V_{max}), respectively. For all inhibition kinetic analysis, goodness-of-fit parameters were employed to identify the most appropriate inhibition modes.

2.5 UV-visible absorption spectra

The UV-visible absorption spectra were recorded by an ultraviolet spectrophotometer (Mapada Instrument Co., Ltd., China) according to the method of Ren with modifications [29]. Briefly, 250 μL of citrate-Na_2HPO_4 buffer (pH 8.0) or PPL (0.1 mg/mL, final concentration) was mixed with 250 μL of different concentrations of the four inhibitors (final concentrations of 50 and 100 μM, respectively) and then allowed to stand for 30 min at 25 ℃ before measurement. Using citrate-Na_2HPO_4 buffer as a reference, the absorption spectra of the PPL solution, inhibitor + lipase complex solution, and inhibitor solution were scanned in a range of 200–400 nm.

2.6 Circular dichroism (CD) measurement

CD spectroscopy was used to determine whether the four PMFs affect the secondary conformation of PPL, and the experiment was performed as described by

Du et al [30]. Mixture solutions of 50 μM of the four inhibitors and 0.1 mg/mL PPL were injected into a 0.1 cm path length quartz cuvette and kept at 25 ℃ for 30 min. Then, each mixture was measured using a Chirascan V100 spectrophotometer (Applied Photophysics, Surrey, UK) at 100 nm/min with a slit width of 1 nm and a time constant of 1 s. Each CD spectra was the accumulation of three times scans. The data were recorded ranging from 200 nm to 260 nm at 1 nm interval and analyzed by CDpro software after deducting the buffer spectrum.

2.7 Fluorescence spectroscopic measurements

The fluorescence spectra were conducted as described by Liu's method with appropriate modifications [31]. In the presence of different concentrations of inhibitor (0, 5, 10, 25, 50, 100, 150 and 200 uM, final concentration), 0.1 mg/mL PPL solution was mixed at room temperature. After 30 min, the mixture was injected into a quartz cuvette and the fluorescence intensity was recorded from 290 nm to 450 nm at an excitation wavelength at 280 nm using a fluorescence spectrophotometer (Hitachi, Japan). The excitation and emission slits were both 5 nm. According to the Stern–Volmer equation, the fluorescence quenching results were plotted as a plot of fluorescence intensity versus inhibitor concentration [32]:

$$F_0/F = 1 + K_q \tau_0 [I] = 1 + K_{SV}[I] \quad (5)$$

where F_0 and F were the fluorescence intensities before and after the addition of the quenchers (PMFs), respectively. Kq, K_{SV}, τ_0, and $[I]$ were the bimolecular quenching constant, the Stern–Volmer dynamic quenching constant, the fluorescence

lifetime in the absence of the quencher (herein τ_0 is 1.59 ns [33]), and the concentration of the quenchers, respectively. K_{sv} could be calculated from the slope of F_0/F against [I], which indicated a dynamic balance of molecular diffusion and collisions and measured the quenching efficiency of effectors on the enzyme.

The mechanism of fluorescence quenching can be divided into two categories: static quenching owing to ground-state complex formation and dynamic quenching owing to collisions between molecules [33]. For the static type, the binding constant (K_A) and the binding site (n) are calculated from the intercept and the slope of lg[(F_0 −F)/F] against lg[I] with the linear regression Eq. (6) [32]:

$$\lg\left[(F_0 - F)/F\right] = \lg K_A + \mathrm{n}\lg\left[I\right] \quad (6)$$

2.8 Molecular docking and MD simulation

TAN (ID: 68077), 5-DT (ID: 96539), NBT (ID: 72344) and 5-DN (ID: 358832) data were downloaded from the PubChem database (https://pubchem.ncbi.nlm.nih.gov/). The crystal structure of pancreatic lipase (PDB: 1LPB) with a resolution of 2.46 Å was obtained from the Research Collaboratory for Structural Bioinformatics (RCSB) Protein Data Bank (http://www.rcsb.org). The PDBQT format files of all above models were generated by the AutoDockTools 1.5.6rc3 software [34]. Then, the AutoDock 4.2 program [34] was used to determine the possible binding sites through a Lamarckian genetic algorithm (LGA). A docking box centered on the Arg265 residue was used in a size of 50 × 30 × 30 $Å^3$, which covered the catalytic center of pancreatic lipase (His263, Ser152, and Phe77). The number of alternative conformations was set to 100. All produced conformations with

respective docking energies (kcal mol^{-1}) were clustered with a tolerance of root-mean-square deviation (RMSD) of 12.0 Å.

Base on the docking results, MD was used to obtain the stable conformation of the pancreatic lipase-NBT complex by Gromacs 2018.3 program [35]. The Gromos96 54a7 force field was applied to a cubical periodic box with a 1.0 nm solute-wall distance, which contained pancreatic lipase complexed with nobiletin filled with SPC/E water and counterions. The energy of the box was optimized using the steepest descent method, with a maximum step of 5000, up to a maximum force F_{max} of no more than 1000.0 kJ mol^{-1} nm^{-1}. Then, the box was equilibrated under the canonical and isothermal-isobaric ensembles. After each equilibration for 100 ps, production runs of 50 ns were performed. The MD results were visualized using the Chimera 1.12 packages [36].

2.9 Statistical analysis

All experiments were implemented in triplicate, and the data are shown as mean ± SD. The IC_{50} values (the concentration of inhibitor that reduces enzyme activity by 50%) were evaluated by nonlinear regression using SPSS statistics software (version 17.0, IBM SPSS Software, Inc., USA).

3. Result and discussion

3.1 Structural identification of the PMFs in citrus peel extract by UPLC-TOF-MS

In this study, TAN (1) and NBT (3) were obtained by extraction with ethyl acetate. 5-DT (2) and 5-DN (4) were obtained by the method already described and

illustrated in Fig. 1. The PMFs were identified by comparing the retention time of UPLC diagram (Figs. 2a-d) and quasi-molecular ions of TOF-MS spectra (Figs. 2a'-d') based on positive ionization mode. The results in Fig. 2a' exhibited molecular ion $[M+H]^+$ at m/z 373, $[M+Na]^+$ at m/z 395, and an isotopic ion $[M+H+1]^+$ at m/z 375; a fragment ion $[M+H-14]^+$ yielding at m/z 358 was attributed to the loss of methylene, which were consistent with the mass spectrometry results reported for TAN [37]. The results indicated in Fig. S1b' displayed molecular ion $[M+H]^+$ at m/z 359 and $[M+Na]^+$ at m/z 381, consistent with the molecular weight of 5-DT (358 Da), and $[M+H+1]^+$ ion at m/z 360, $[M+H+2]^+$ ion at m/z 361, and $[M+H+3]^+$ ion at m/z 362 were corresponding to the isotope atom present in 5-DT [38]. The spectrum shown in Fig. 2c' could be tentatively identified as NBT based on $[M+H]^+$ ion at m/z 403, $[M+Na]^+$ ion at m/z 425, and isotopic ion clusters of $[M+H+1]^+$ at m/z 404 and $[M+H+2]^+$ at m/z 405 [39]. The spectrum shown in Fig. S1d' was possibly 5-DN with $[M+H]^+$ ion at m/z 389 and $[M+Na]^+$ ion at m/z 411. $[M+H+1]^+$ ion at m/z 390 and $[M+H+2]^+$ ion at m/z 391 were considered to be isotopic molecular ions [38]. Therefore, in combination with chromatograms and mass spectra, the four PMFs could be identified in turn as TAN (RT 5.30 min, 372 Da), 5-DT (RT 5.99 min, 358 Da), NBT (RT 4.89 min, 402 Da), and 5-DN (RT 5.57 min, 388 Da), which were further investigated for the PPL inhibition experiments.

3.2 Real-time inhibition of lipase by the four kinds of PMFs

Citrus fruits are widely distributed and consumed around the world and are an

essential part of the Mediterranean diet [40]. Our research determined the inhibitory potentials of TAN, 5-DT, NBT, and 5-DN against PPL by the fluorometric method using 4-MU oleate as the substrate to evaluate the inhibitory activity of the PMFs on lipase *in vitro*. The 3-dimensional (3D) surface heat map (Figs. 3a-3d) was adopted to provide an intuitive and comprehensive presentation of the real-time inhibition trend of the four PMFs on PPL at different concentrations within 35 min. In the range of concentrations (0, 5, 10, 15, 25, 50, 100 and, 200 μM, final concentration) investigated, the inhibition surface heat map gradually changed from blue (low inhibitory activity) to red (high inhibitory activity), indicating that the catalytic activities of PPL were inhibited by the PMFs in a dose-dependent manner. The same results were shown in the residual activity curves (Fig. 3e), the residual activity of PPL decreased with the increasing concentration of the four inhibitors. When the inhibitor concentration increased to 50 μM, the effects of the four PMFs on PPL activity gradually reached the plateau stage. As shown in Table 1, the inhibitory capacity of NBT on PPL was 4.08 times higher than that of TAN, and the inhibitory capacity of 5-DN on PPL was 3.15 times higher than that of 5-DT. The result may be associated with the existence of one more hydrophobic methoxy group at the 3′-position of the B ring of NBT and 5-DN compared with TAN and 5-DT, which improved their ability to bind to the hydrophobic region of the lipase surface [41] and exerted better PPL inhibition effects, whereas, there was no significant difference in PPL inhibitory activities between 5-DT or 5-DN and their precursor compounds (p>0.05). This result may suggest that the group at the 5-position of the PMFs,

whether it was a hydroxyl group or a methoxy group, had no significant effect on the inhibition of lipase activity (p>0.05). As can be seen from Table 1 and Fig. 3e, NBT had the most potent inhibitory capacity (IC_{50} value of minimum) against PPL among the four PMFs, which may confirm the inference made in our previous study [24]. Although many naturally derived flavonoids have been investigated for their potential anti-lipase activities [27, 42, 43], it was evident from our study that TAN, 5-DT, NBT, and 5-DN displayed remarkably stronger inhibitory effects on PPL than that of the other flavonoids (hesperidin, *Nelumbo nucifera* leaf flavonoids, apigenin and its glycosides, etc.), which made them promising candidates for their application as natural lipase inhibitors.

3.3 Inhibitory kinetics of the four PMFs on PPL

There are four types of enzyme inhibition mechanisms: competitive inhibition, non-competitive inhibition, uncompetitive inhibition, and linear mixed inhibition [30]. To investigate the inhibitory mechanisms of the four PMFs on PPL, kinetic studies were implemented with the initial reaction rates over different concentrations of 4-MU oleate in the absence or presence of TAN, 5-DT, NBT, and 5-DN (0, IC_{50}, and $2IC_{50}$, final concentration). As shown in Figs. 4a-d, with an increase in substrate concentration, the enzymatic reaction rate was firstly positively correlated with the substrate concentration, and then gradually tended to the maximum reaction rate. The Lineweaver-Burk double reciprocal plots in terms of 1/v versus 1/[*S*] were shown in Figs. 4a'-4d'. These double reciprocal plots produced a set of straight lines that

converged to a point in the third quadrant, indicating that the four PMFs exhibited reversible mixed-type inhibition on PPL [44]. Namely, the four PMFs were able to form enzyme-inhibitor and enzyme-substrate-inhibitor complexes regardless of whether a substrate molecule could bind with the enzyme active site or not [45], which was different from orlistat forming a covalent bond with a serine residue at the lipase active site [46]. Previous research has reported lipase inhibitors of natural polyphenols and flavonoids, such as cocoa procyanidins [47], blackberry polyphenols [48], polyphenols of cortex mori radices [44], and ginkgo biloba flavonoids [28] also had mixed inhibition mechanisms. This indicated that these natural lipase inhibitors could bind to the active site and the inactive center of the enzyme to exhibit a dual inhibitory ability. The K_i value, a dissociation constant of inhibitors binding with enzyme, is an important parameter to evaluate the affinity between lipase and the inhibitor [28]. In this research, the K_i values of TAN, 5-DT, NBT, and 5-DN were calculated, which were listed in Table 2. Compared with the K_i values of TAN and 5-DT, the K_i values of NBT and 5-DN presented a significant difference (p<0.05). According to the mixed inhibition Eq. (4), when the K_i value decreased, the initial rate of the reaction decreased, and the binding of the enzyme to the inhibitor weakened the binding of the enzyme to the substrate. Therefore, the smaller the K_i value, the stronger the binding between the enzyme and the inhibitor, and the stronger the inhibitory activity [49]. Therefore, our results further verified the real-time inhibition rate of lipase, and NBT and 5-DN were potent mixed-type inhibitors against PPL, with K_i values <4 μM.

3.4 UV-visible absorption spectra

UV-visible spectroscopy was applied in this study to confirm the structural changes in PPL when combined with the PMFs. UV absorption alterations of the chromophore in constituent amino acids can reflect changes in the structure and stability of the protein [50, 51]. Figs. 6a-6d showed the absorption spectra curves of lipases in the presence of TAN, 5-DT, NBT, and 5-DN at different concentrations (PMFs + Lipase) while curves shown in Figs. 6a'-6d' were obtained by deducting the PMFs UV absorbance from PMFs + Lipase spectra curves. Two absorption peaks of PPL at 219 nm and 267 nm got stronger with the increasing inhibitor concentration. The strong absorption peak at 219 nm reflected the frame structure of the lipase [29]; the weaker absorption peak at 267 nm was the UV absorption of the aromatic amino acids of the lipase (mainly of Trp and Tyr). The change in the absorption peak indicated conformation alterations in PPL. In the absence of interaction between the four inhibitors and PPL, the PMF + Lipase curves should coincide with the PPL curves. It can be seen from Figs. 6a'-6d' that the absorption peak at 267 nm had a significant change for varying degree of redshift occurred after the addition of inhibitors. The result suggested that the PMFs and PPL formed a new complex and this complex altered the structural conformation of PPL, thereby affecting the microenvironment around its Trp and Tyr residues and increasing or decreasing the UV absorbance.

3.5 Circular dichroism (CD) of PPL

CD is a sensitive optical technique that has been widely used to study the optical

conformational properties of various biological and synthetic macromolecules [52]. CD spectroscopy is commonly employed for the analysis of protein secondary structures [53]. The CD spectra of PPL in the presence of different inhibitors were shown in Fig. 5. Two negative peaks can be seen near 208 nm and 228 nm in the spectra of PPL without inhibitors, which could be attributed to the α-helix of PPL [54]. All the spectra showed great differences with the addition of the inhibitors although the position of the negative peaks did not change significantly. The result indicated that PPL still retained an α-helical structure, but its normal secondary structure was affected.

The CDpro software was used to measure the secondary structure of PPL in the presence and absence of inhibitors. As shown in Table 2, the main secondary conformation of PPL without inhibitors was α-helix (10%), β-sheet (32%), β-turn (23%), and unordered (36.6%). However, with the addition of TAN, 5-DT, NBT, or 5-DN, both the percentages of α-helix and β-turn of PPL decreased while the percentage of β-sheet increased significantly. This indicated that the four PMFs had a certain degree of binding with the active site of PPL comprising α-helix [55], resulting in a decrease in structural stability and inhibition of substrate decomposition activity [56]. It has been reported that the 449 amino acid residues of PPL were arranged in the N-terminal domain with typical α/β structure and C-terminal domain with a β-sandwich structure [55]. The decrease in α-helix and the increase in β-sheet shown in Table 2 may represent the inhibition degree of PPL by the four PMFs. NBT showed the greatest modification in the content of α-helix (5.1%), β-sheet (64.1%), and β-turn

(16.1%) in PPL among the four inhibitors, which may suggest that NBT had a better inhibitory effect on PPL than that of TAN, 5-DT, and 5-DN. This result was consistent with the inhibition rate and kinetics of NBT on PPL.

3.6 Fluorescence spectroscopy

Fluorescence spectroscopy is a promising method for studying the interaction between small molecules and proteins and has been widely used in structural studies of functional proteins to reflect changes in the microenvironment of protein fluorophores [57]. Seven Trp residues (five at N-terminal domain, two at C-terminal domain, among them, three Trp residues near the active site of the enzyme), 25 Phe residues, and 16 Tyr residues may be responsible for the PPL fluorescence and provide conformational information about the binding between small molecules and PPL [58]. The fluorescence spectra of PPL in the presence of different concentrations of the four PMFs (0, 5, 10, 25, 50, 100, 150, 200 μM, final concentration) were shown in Figs. 7a-d. With the increase of PMF concentration, the fluorescence intensity of PPL decreased, accompanied by a redshift of the maximum emission peak (357 nm). Furthermore, the maximum absorption peak of NBT shown in Fig. 7c was the most obvious. This result indicated that the interaction between NBT and the fluorophore (such as tryptophan) at the active site of PPL or other sites was stronger than that of the three other PMFs, thus changing the original conformation of PPL and the microenvironment around the fluorophore and leading to fluorescence quenching [33].

The mechanism of PPL fluorescence quenching induced by these PMFs can be analyzed by the Stern-Volmer plot equation. Either in dynamic or static quenching, F_0/F is a linear relationship to [I], while mixed quenching is an upward curve towards the y-axis [59]. A good linear relationship (R^2>0.98) of TAN, 5-DT, and 5-DN was observed in Fig. 7e and Table 2, while an upward curvature towards the Y-axis of NBT was observed when the concentration was higher than 100 μM. These results suggested the existence of a mixed quenching process at high concentrations. In addition, the fluorescence quenching constant (K_{sv}) and binding affinity (K_q) of NBT were significantly higher than those of the other three compounds (p<0.01), indicating that NBT had better PPL binding ability than that of the other three PMFs. It has been reported that the maximum scattering collision quenching constant of different quenchers and biopolymers for dynamic quenching was 2.0×10^{10} $L\cdot M^{-1}\cdot s^{-1}$ [60]. Therefore, the combination of these four inhibitors with PPL was not a dynamic quenching process. Finally, the binding constants (K_A) and binding sites (n) of the four PMFs to PPL could be accurately calculated by the intercept and slope of the double logarithmic Eq. (6) (Fig. 7f). From the results listed in Table 2, it can be seen that the order of K_A values of the four inhibitors on PPL was NBT>5-DN>TAN>5-DT>10^3 L mol^{-1}, which indicated their efficiency in binding with PPL. Noteworthy, the affinity of NBT to PPL was much higher than that of the other three inhibitors. The data for binding sites (n) indicated that the four inhibitors had one common binding site with PPL. The result suggested that PMFs may form a ground-state complex with a fluorescent group, such as tryptophan at the PPL active site, thereby diminishing the

ability of PPL to decompose the substrate. Our results also illustrated that the binding of the four PMFs to PPL caused a change in the structure and the catalytic activity of the protein. These also further validated the results of inhibition kinetics, CD, and UV-visible spectra.

3.7 Molecular docking

The molecular docking simulations were performed to investigate the inhibitory behaviors of the four PMFs against PPL-mediated 4-MU oleate hydrolysis from the view of ligand-enzyme interactions [61]. Fig. 8 showed the spatial conformation of the inhibitor-enzyme complex after the docking of TAN, 5-DT, NBT, and 5-DN with PPL. As it can be seen from Fig. 8, there were two sites on PPL for binding of the PMFs: one near the active site (binding site 1), strongly interacting with the His263, Ser152, Phe77, and Arg256 residues (Figs. 8a-d) and the other (binding site 2) far away from the active center (Figs. 8a'-d'). This result was consistent with the inhibitory kinetic analysis of the mixed inhibition type. As shown in Fig. 8, the four PMFs interacted with Tyr114 and Phe77 at docking site 1 (a-b) and Tyr369 at docking site 2 (a'-b'), which directly quenched the endogenous fluorescence of PPL. This further confirmed the results of the PPL fluorescence quenching experiment. Molecular docking energy corresponds to the affinity between small molecules and proteins; the lower the energy, the more stable is the ligand-protein complex structure [62, 63]. In terms of the docking energy (Table 4), the four compounds were preferentially bound to the active center (site 1), with docking energies of -6.22, -6.26,

-6.60, and -6.21 kcal mol^{-1}, respectively. Among them, the affinity of NBT to PPL was higher than that of the other three compounds in binding sites 1 and 2, which was consistent with the IC_{50} value and the binding affinity constant (K_q) of fluorescence quenching. Moreover, in addition to a few hydrogen bonds, there were a lot of hydrophobic interactions between the four PMFs and the residues of the two active sites in the lipase (Fig. 8). These results further confirmed that the inhibitory effect of the PMFs on the lipase was related to its structural methoxy group [64]. In addition, the molecular docking analysis again proved that the four PMFs mainly inhibited the substrate decomposition activity of lipase by hydrophobic interactions with lipase activation site (site 1) and inactivation site (site 2). Thus, the interaction between NBT and PPL was stronger than that of the other three PMFs with PPL.

3.8 MD simulation

In order to further understand the mixed inhibitory effect of the PMFs on PPL, the MD technique was used to explore the detailed structural information of the NBT-PPL complex, using NBT as a representative compound. In the MD simulation, the root mean square deviation (RMSD) of the protein structure as a function of time is an important measurement to monitor the equilibrium process of the system and the stability of protein structure upon the binding of a ligand, and the RMSD is used to assess structural deviation from the initial protein structure [60, 65-67]. As shown in Fig 9a, the fluctuation of RMSD was less than 0.2 nm, indicating that PPL had reached a stable state in both NBT and water systems within 50 ns [68]. The radius of

rotation (Rg) is an important parameter to investigate the compactness of the protein structure in the process of simulation. The larger the Rg value of the system, the larger the radius of the rotation range of the protein structure in a certain space, and the looser the protein structure [60]. The Rg value obtained (Fig. 9b) showed that the binding of NBT increased the Rg of PPL, indicating that NBT could unfold the enzyme to loose the whole conformation. In other words, the greater the binding energy of PMFs to lipase, the more unstable its structure, thereby leading to the loss of catalytic activity of the functional site of lipase [69]. This also confirmed the results of UV-Visible and CD spectra. Fig. 9e showed the solvation stable conformation of PPL and NBT-PPL complexes obtained by MD analysis. From the conformational diagram in Fig. 9e, it can be seen that NBT had two binding sites on PPL, which was consistent with the results of the kinetic studies and molecular docking. In addition, the results obtained from Figs. 9c and 9d revealed that the hydrophobic forces dominated the interaction between NBT and residues at the catalytic center (site 1) and non-catalytic center (site 2). This result further confirmed our previous inference that the inhibitory effect of PMFs on lipase could be related to the location and number of methoxy groups (hydrophobic groups) in its structure [64].

4. Conclusion

Obesity has become a global public health problem. The development of food-borne small molecule compounds as effective inhibitors of pancreatic lipases can not only replace chemical drugs, avoiding adverse reactions, but also provide theoretical

support for reasonable adjustment of dietary habits. In this study, UV-visible spectroscopy, CD spectroscopy, fluorescence spectroscopy, molecular docking, and MD simulation, among other methods, were employed to investigate the inhibitory mechanism and structure-activity relationship of TAN, 5-DT, NBT, and 5-DN on PPL. The results showed that these PMFs may be able to change the spatial structure of PPL through hydrophobic bond to form a complex, which affected the original conformation and active site of PPL. Our results suggest that the inhibition of lipase by the PMFs was mainly due to the methoxy group (hydrophobic group) at the 3′-position of the B ring. Furthermore, compared with the three other PMFs, NBT had the best inhibitory effect on PPL and is expected to be a novel PPL inhibiting drug precursor. Overall, this study provides basic data supporting the development of anti-obesity functional foods.

Conflicts of interest

There are no conflicts of interest to declare.

Acknowledgments

This work was financially supported by national food science and engineering first-class discipline construction project (NO.JUFSTR20180204), The national key research and development plan in the 13th Five-Year (NO.2017YFD0400803).

References

[1] T.J. Little, M. Horowitz, C. Feinle-Bisset, Am J Clin Nutr, 86 (2007) 531-541.

[2] P.E.S.F. Ali H. Mokdad, MD, MPH; Barbara A. Bowman, PhD; William H. Dietz, MD, PhD; Frank Vinicor, MD, MPH; Virginia S. Bales, MPH; James S. Marks, MD, MPH JAMA-JOURNAL OF THE AMERICAN MEDICAL ASSOCIATION, 289 (2003) 76-79.

[3] P.P. Marie-Eve Piché, Isabelle Lemieux, Jean-Pierre Després, Progress in Cardiovascular Diseases, 61

(2018) 103-113.
[4] K. Wang, X.-h. Yu, Y.-J. Tang, Y.-l. Tang, X.-h. Liang, Life sciences, 233 (2019).
[5] V.I.K. Boyd A Swinburn, Steven Allender, Vincent J Atkins, Phillip I Baker, Jessica R Bogard, Hannah Brinsden, Alejandro Calvillo, Olivier De Schutter, Raji Devarajan, Majid Ezzati, Sharon Friel, Shifalika Goenka, Ross A Hammond, Gerard Hastings, Corinna Hawkes, Mario Herrero, Peter S Hovmand, Mark Howden, Lindsay M Jaacks, Ariadne B Kapetanaki, Matt Kasman, Harriet V Kuhnlein, Shiriki K Kumanyika, Bagher Larijani, Tim Lobstein, Michael W Long, Victor K R Matsudo, Susanna D H Mills, Gareth Morgan, Alexandra Morshed, Patricia M Nece, An Pan, David W Patterson, Gary Sacks, Meera Shekar, Geoff L Simmons, Warren Smit, Ali Tootee, Stefanie Vandevijvere, Wilma E Waterlander, Luke Wolfenden, William H Dietz, The Lancet, 393 (2019) 791-846.
[6] K.E. Foster-Schubert, D.E. Cummings, Endocrine reviews, 27 (2006) 779-793.
[7] P.B. Yuguang Shi, Nature Reviews Drug Discovery, 3 (2004) 695-710.
[8] K.S. McClendon, D.M. Riche, G.I. Uwaifo, Expert Opin Drug Saf, 8 (2009) 727-744.
[9] M.D.A. Homayoun L. Daneschvar, Gerald W. Smetana, The American Journal of Medicine, 129 (2016) 879.e871-879.e876.
[10] T.T.C.a.N.R.S. Bernard Man Yung Cheung, Therapeutic Advances in Drug Safety, 4 (2013) 171-181.
[11] T.T. Sham, C.O. Chan, Y.H. Wang, J.M. Yang, D.K. Mok, C.W. Chan, BioMed research international, 2014 (2014) 925302.
[12] D. Song, L. Cheng, X. Zhang, Z. Wu, X. Zheng, Journal of food biochemistry, 43 (2019) e12954.
[13] E. Kato, Biosci Biotechnol Biochem, 83 (2019) 975-985.
[14] T. Buchholz, M.F. Melzig, Planta medica, 81 (2015) 771-783.
[15] D.R. Goncalves, J.A. Manthey, P.I. da Costa, M.C.M. Rodrigues, T.B. Cesar, Journal of agricultural and food chemistry, 66 (2018) 7531-7541.
[16] H.H. Arab, W.R. Mohamed, B.M. Barakat, S.A. Arafa el, Chem Biol Interact, 258 (2016) 205-213.
[17] M. Fu, Y. Xu, Y. Chen, J. Wu, Y. Yu, L. Zou, K. An, G. Xiao, Food Chem, 230 (2017) 649-656.
[18] Y.S. Lee, B.Y. Cha, S.S. Choi, B.K. Choi, T. Yonezawa, T. Teruya, K. Nagai, J.T. Woo, J Nutr Biochem, 24 (2013) 156-162.
[19] R. Sundaram, P. Shanthi, P. Sachidanandam, Journal of Functional Foods, 16 (2015) 315-333.
[20] E.M. Kurowska, J.A. Manthey, Journal of agricultural and food chemistry, 52 (2004) 2879-2886.
[21] L.A. Nichols, D.E. Jackson, J.A. Manthey, S.D. Shukla, L.J. Holland, Lipids in health and disease, 10 (2011) 36.
[22] J.M. Assini, E.E. Mulvihill, M.W. Huff, Current opinion in lipidology, 24 (2013) 34-40.
[23] Y.-S. Lee, B.-Y. Cha, K. Saito, H. Yamakawa, S.-S. Choi, K. Yamaguchi, T. Yonezawa, T. Teruya, K. Nagai, J.-T. Woo, Biochemical pharmacology, 79 (2010) 1674-1683.
[24] S.L. Zeng, S.Z. Li, C.J. Lai, M.Y. Wei, B.Z. Chen, P. Li, G.D. Zheng, E.H. Liu, Phytomedicine : international journal of phytotherapy and phytopharmacology, 43 (2018) 103-109.
[25] X. Huang, X. Kou, L. Wang, R. Ji, C. Ma, H. Wang, Lwt, (2019) 108469.
[26] Z. Gao, W. Gao, S.-L. Zeng, P. Li, E.H. Liu, Journal of Functional Foods, 40 (2018) 498-509.
[27] K. Kawaguchi, T. Mizuno, K. Aida, K. Uchino, Bioscience, biotechnology, and biochemistry, 61 (1997) 102-104.
[28] P.K. Liu, Z.M. Weng, G.B. Ge, H.L. Li, L.L. Ding, Z.R. Dai, X.D. Hou, Y.H. Leng, Y. Yu, J. Hou, International journal of biological macromolecules, 118 (2018) 2216-2223.
[29] G. Ren, H. Sun, J. Guo, J. Fan, G. Li, S. Xu, Food Funct, (2019).
[30] X. Du, M. Bai, Y. Huang, Z. Jiang, F. Chen, H. Ni, Q. Li, Journal of Functional Foods, 48 (2018)

551-557.
[31] T.T. Liu, X.R. He, R.X. Xu, X.B. Wu, Y.X. Qi, J.Z. Huang, Q.H. Chen, Q.X. Chen, International journal of biological macromolecules, 120 (2018) 1925-1934.
[32] Y.-Q. Wang, H.-M. Zhang, G.-C. Zhang, W.-H. Tao, S.-H. Tang, Journal of luminescence, 126 (2007) 211-218.
[33] S. Wang, S. Dong, R. Zhang, H. Shao, Y. Liu, Process Biochemistry, 49 (2014) 237-243.
[34] G.M. Morris, R. Huey, W. Lindstrom, M.F. Sanner, R.K. Belew, D.S. Goodsell, A.J. Olson, Journal of computational chemistry, 30 (2009) 2785-2791.
[35] P. S, P. S, S. R, L. P, B. P, A. R, S. MR, S. JC, K. PM, v.d.S. D, H. B, L. E, Bioinformatics, 29 (2013) 845-854.
[36] E.F. Pettersen, T.D. Goddard, C.C. Huang, G.S. Couch, D.M. Greenblatt, E.C. Meng, T.E. Ferrin, J Comput Chem, 25 (2004) 1605-1612.
[37] D.-Y. Zhou, Q. Xu, X.-Y. Xue, F.-F. Zhang, X.-M. Liang, Journal of pharmaceutical and biomedical analysis, 49 (2009) 207-213.
[38] B. Weber, B. Hartmann, D. Stöckigt, K. Schreiber, M. Roloff, H.-J. Bertram, C.O. Schmidt, Journal of agricultural and food chemistry, 54 (2006) 274-278.
[39] H.-F. Chen, W.-G. Zhang, J.-B. Yuan, Y.-G. Li, S.-L. Yang, W.-L. Yang, Journal of pharmaceutical and biomedical analysis, 59 (2012) 90-95.
[40] J.A.S. Suryawanshi, African Journal of Plant Science, 5 (2011) 390-395.
[41] P. Reis, K. Holmberg, H. Watzke, M. Leser, R. Miller, Advances in colloid and interface science, 147 (2009) 237-250.
[42] S. Liu, D. Li, B. Huang, Y. Chen, X. Lu, Y. Wang, J Ethnopharmacol, 149 (2013) 263-269.
[43] R. Atma, Y. Takahashi, K. Yamaki, Food Research International, 75 (2015) 289-294.
[44] X.D. Hou, G.B. Ge, Z.M. Weng, Z.R. Dai, Y.H. Leng, L.L. Ding, L.L. Jin, Y. Yu, Y.F. Cao, J. Hou, Bioorganic chemistry, 80 (2018) 577-584.
[45] A.T. Girgih, C.C. Udenigwe, H. Li, A.F. Adebiyi, R.E. Aluko, Journal of the American Oil Chemists' Society, 88 (2011) 1767-1774.
[46] J.W. Yun, phytochemistry, 71 (2010) 1625-1641.
[47] Y. Gu, W.J. Hurst, D.A. Stuart, J.D. Lambert, Journal of agricultural and food chemistry, 59 (2011) 5305-5311.
[48] D. Sosnowska, A. Podsędek, M. Redzynia, A.Z. Kucharska, Journal of Functional Foods, 49 (2018) 196-204.
[49] L.H. Wei, T.R. Chen, H.B. Fang, Q. Jin, S.J. Zhang, J. Hou, Y. Yu, T.Y. Dou, Y.F. Cao, W.Z. Guo, G.B. Ge, International journal of biological macromolecules, 134 (2019) 622-630.
[50] Q. Yang, J. Liang, H. Han, The Journal of Physical Chemistry B, 113 (2009) 10454-10458.
[51] S. Sadeghi-Kaji, B. Shareghi, A.A. Saboury, S. Farhadian, International journal of biological macromolecules, 131 (2019) 473-483.
[52] T. Osterlund, D.J. Beussman, K. Julenius, P.H. Poon, S. Linse, J. Shabanowitz, D.F. Hunt, M.C. Schotz, Z.S. Derewenda, C. Holm, Journal Of Biological Chemistry, 274 (1999) 15382-15388.
[53] L. Whitmore, B.A. Wallace, Biopolymers: Original Research on Biomolecules, 89 (2008) 392-400.
[54] M. Ying, M.D. Meti, H. Xu, Y. Wang, J. Lin, Z. Wu, Q. Han, X. Xu, Z. He, W. Hong, Z. Hu, International journal of biological macromolecules, 120 (2018) 1345-1352.
[55] F. Winkler, A. d'Arcy, W. Hunziker, Nature, 343 (1990) 771.
[56] J.D. Schrag, Y. Li, S. Wu, M. Cygler, Nature, 351 (1991) 761.

[57] L. Sun, W. Chen, Y. Meng, X. Yang, L. Yuan, Y. Guo, F.J. Warren, M.J. Gidley, Food Chem, 208 (2016) 51-60.
[58] A.I. Martinez-Gonzalez, E. Alvarez-Parrilla, A.G. Diaz-Sanchez, L.A. de la Rosa, J.A. Nunez-Gastelum, A.A. Vazquez-Flores, G.A. Gonzalez-Aguilar, Food technology and biotechnology, 55 (2017) 519-530.
[59] K.L. Zhou, D.Q. Pan, Y.Y. Lou, J.H. Shi, Journal of molecular recognition : JMR, 31 (2018) e2716.
[60] L. Zhang, P. Wang, Z. Yang, F. Du, Z. Li, C. Wu, A. Fang, X. Xu, G. Zhou, Food Hydrocolloids, (2019) 105455.
[61] T. Lengauer, M. Rarey, Current opinion in structural biology, 6 (1996) 402-406.
[62] G.K. Veeramachaneni, K.K. Raj, L.M. Chalasani, S.K. Annamraju, B. JS, V.R. Talluri, Bioinformation, 11 (2015) 535.
[63] S.K. Saha, P. Banerjee, Materials Chemistry Frontiers, 2 (2018) 1674-1691.
[64] H. Sato, V.T.G. Chuang, K. Yamasaki, N. Yamaotsu, H. Watanabe, K. Nagumo, M. Anraku, D. Kadowaki, Y. Ishima, S. Hirono, PloS one, 9 (2014) e87919.
[65] H. Monhemi, M.R. Housaindokht, A. Nakhaei Pour, The journal of physical chemistry. B, 119 (2015) 10406-10416.
[66] G. Palermo, L. Casalino, A. Magistrato, J. Andrew McCammon, Journal of structural biology, 206 (2019) 267-279.
[67] Z. Chen, J. Pei, R. Li, F. Xiao, Construction and Building Materials, 189 (2018) 695-710.
[68] Ni, C.A. Sotriffer, J.A. McCammon, Journal of medicinal chemistry, 44 (2001) 3043-3047.
[69] S.K. Saha, M. Murmu, N.C. Murmu, I.B. Obot, P. Banerjee, Surfaces and Interfaces, 10 (2018) 65-73.

Author statement

Xin Huang: Investigation, Data Curation, Writing-Original draft preparation; **Junxiang Zhu:** Software, Methodology; **Li Wang:** Formal analysis; **Huijuan Jing:** Visualization, Writing-Review & Editing; **Chaoyang Ma:** Methodology; **Xingran Kou:** Writing-Review & Editing; **Hongxin Wang:** Resources, Conceptualization, Funding acquisition.

Table 1 The IC_{50} values, K_i values and the inhibition types of four PMFs against PPL-mediated 4-MU oleate hydrolysis.

Compounds	MW	IC_{50} (μM)	K_i (μM)	The type of inhibition	Goodness of fit (R^2)
TAN	372.37	14.69±0.82	8.53±1.77	Mix	0.995
5-DT	358.37	13.18±0.44	10.65±3.59	Mix	0.996
NBT	402.39	3.60±0.19	9.51±1.63	Mix	0.991
5-DN	388.39	4.18±0.26	18.65±5.12	Mix	0.988

PMFs, polymethoxylated flavones; PPL, porcine pancreatic lipase; 4-MU, 4-methylumbelliferyl; MW, molecular weight.

Table 2 Secondary structural contents of PPL (0.1 mg/mL) in four kind of PMFs (50 μM).

Compounds	α-helix (%)	β-sheet (%)	β-turn (%)	Unordered (%)
PPL	10	32	23	36.6
TAN	6.4	53.2	18.9	32.2
5-DT	5.5	63.2	17.2	37.5
NBT	5.1	64.1	16.1	36.8
5-DN	5.4	61.6	17.2	37.2

PMFs, polymethoxylated flavones; PPL, porcine pancreatic lipase.

Table 3 Constants of Stern - Volmer curve of fluorescence quenching and binding constant and site of 4 PMFs on PPL

Compounds	Constants of Stern–Volmer curve			Binding constant and site		
	K_{SV} (10^4 L· mol^{-1})	K_q (10^{12} L·mol^{-1} ·S^{-1})	R^2	n	K_A (L· mol^{-1})	R^2
TAN	1.49±0.30^{bB}	9.36±1.90^{bB}	0.9843	0.7[illegible]±0.04^{D}	1.74×10^4±2.67^{cC}	0.9827
5-DT	0.72±0.09^{cC}	4.50±0.57^{cC}	0.9848	1.0[illegible]±0.10^{cC}	1.63×10^3±1.53^{dD}	0.9535
NBT	9.90±1.23^{aA}	62.28±4.03^{aA}	0.9773	1.43±0.02^{aA}	7.03×10^6±1.20^{aA}	0.9990
5-DN	0.50±0.05^{dC}	3.15±0.29^{dC}	0.9940	1.34±0.05^{bB}	1.33×10^5±1.61^{bB}	0.9928

Note: The data with different capital letters in same column show extremely significant difference($p<0.01$); the data with different little letters in same column show significant difference($p<0.05$).

PMFs, polymethoxylated flavones; PPL, porcine pancreatic lipase.

Table 4 Docking energy of four PMFs at two lipase binding sites.

Compounds	IC_{50} (μM)	Docking energy (kcal mol^{-1})	
		binding site 1	binding site 2
TAN	14.69	−6.22	−3.64
5-DT	13.18	−6.26	−3.97
NBT	3.60	−6.60	−4.05
5-DN	4.18	−6.21	−4.06

PMFs, polymethoxylated flavones

Figures Captions

Fig. 1 Structure diagram of 5-position hydroxylation catalyzed by acid for PMFs. PMFs, polymethoxylated flavones.

Fig. 2 HPLC and UPLC-TOF-MS of TAN (a, a'), 5-DT (b, b'), NBT (c, c') and 5-DN (d, d').

Fig. 3 The 3-dimensional (3D) surface heat maps of the real time-inhibition of TAN (a), 5-DT (b), NBT (c) and 5-DN (d) on PPL, and the residual activity curves (e) of PPL inhibited by the different concentrations (0, 5, 10, 15, 25, 50, 100 and 200 μM) four PMFs at 35 minutes. PPL, porcine pancreatic lipase.

Fig. 4 The inhibitory effects of four natural PPL inhibitors (inhibition concentration of 0, IC_{50} and $2IC_{50}$). The inhibition kinetic curves of TAN (a), 5-DT (b), NBT (c) and 5-DN (d) against PPL mediated 4-MU oleate hydrolysis; the Lineweaver-Burk plots of TAN (a'), 5-DT (b'), NBT (c') and 5-DN (d') against PPL-mediated 4-MU oleate hydrolysis. All data were shown as mean ± SD. PMFs, polymethoxylated flavones; PPL, porcine pancreatic lipase; 4-MU, 4-methylumbelliferyl.

Fig. 5 The CD spectra of PPL in the absence and presence of 4 PMFs. PMFs, polymethoxylated flavones; PPL, porcine pancreatic lipase.

Fig. 6 UV-Vis spectra of PPL, PMF, PMF + PPL of TAN (a), 5-DT (b), NBT (c) and 5-DN (d); UV-Vis spectra of PPL and (PMF + PPL)-PMFs of TAN (a'), 5-DT (b'), NBT (c') and 5-DN (d') at 240-300 nm. PMFs, polymethoxylated flavones; PPL, porcine pancreatic lipase.

Fig. 7 Fluorescence spectra of the different concentrations (0, 5, 25, 50, 100, 150 and

200 μM) TAN (a), 5-DT (b), NBT(c) and 5-DN(d) against PPL; e. Stern-Volmer plot for the PMFs-induced quenching of the intrinsic fluorescence of PPL at 25℃; d. Plots of F_0/F for PPL against [I] of 4 PMFs. PMFs, polymethoxylated flavones; PPL, porcine pancreatic lipase.

Fig. 8 Molecular docking conformations of four PMFs with lipases. a-d and a'-d' is a 2-dimensional (2D) diagram of the interaction between TAN, 5-DT, NBT, 5-DN and the residues at the lipase catalytic center (site 1) and the non-catalytic center (site 2), respectively.

Fig. 9 Molecular dynamics simulation of NBT and PPL. a. RMSD of main chain atoms of PPL as a function of time; b. RG of PPL and PPL-NBT complex; c and d. The stereo positional relationship between NBT and residues of PPL at binding sites 1 and 2; e. Stable conformation of the PPL-NBT complex after 50 ns.

Fig. 1

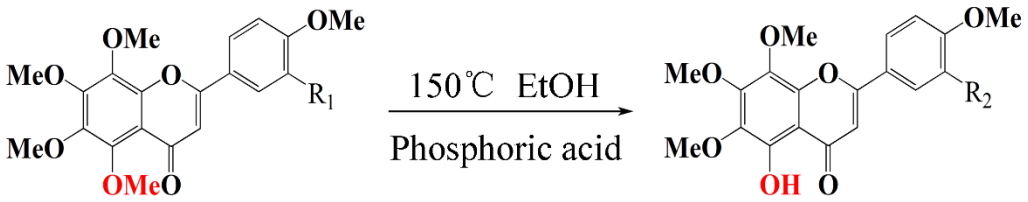

(1) Tangeretin R_1=H

(2) 5-Demethyltangeretin R_2=H

(3) Nobiletin R_1=OMe

(4) 5-Demethylnobiletin R_2=OMe

Fig. 2

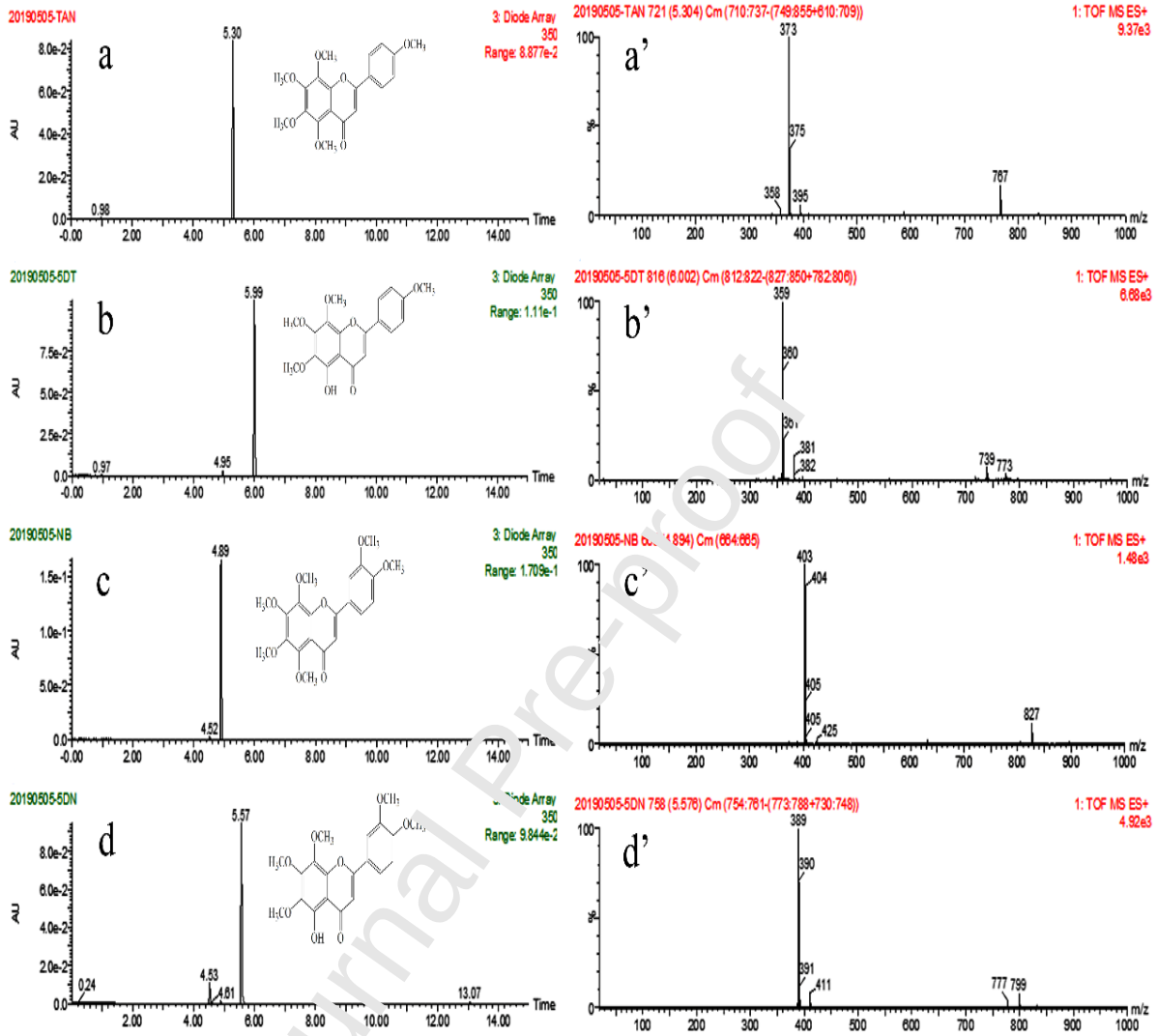

Fig. 3

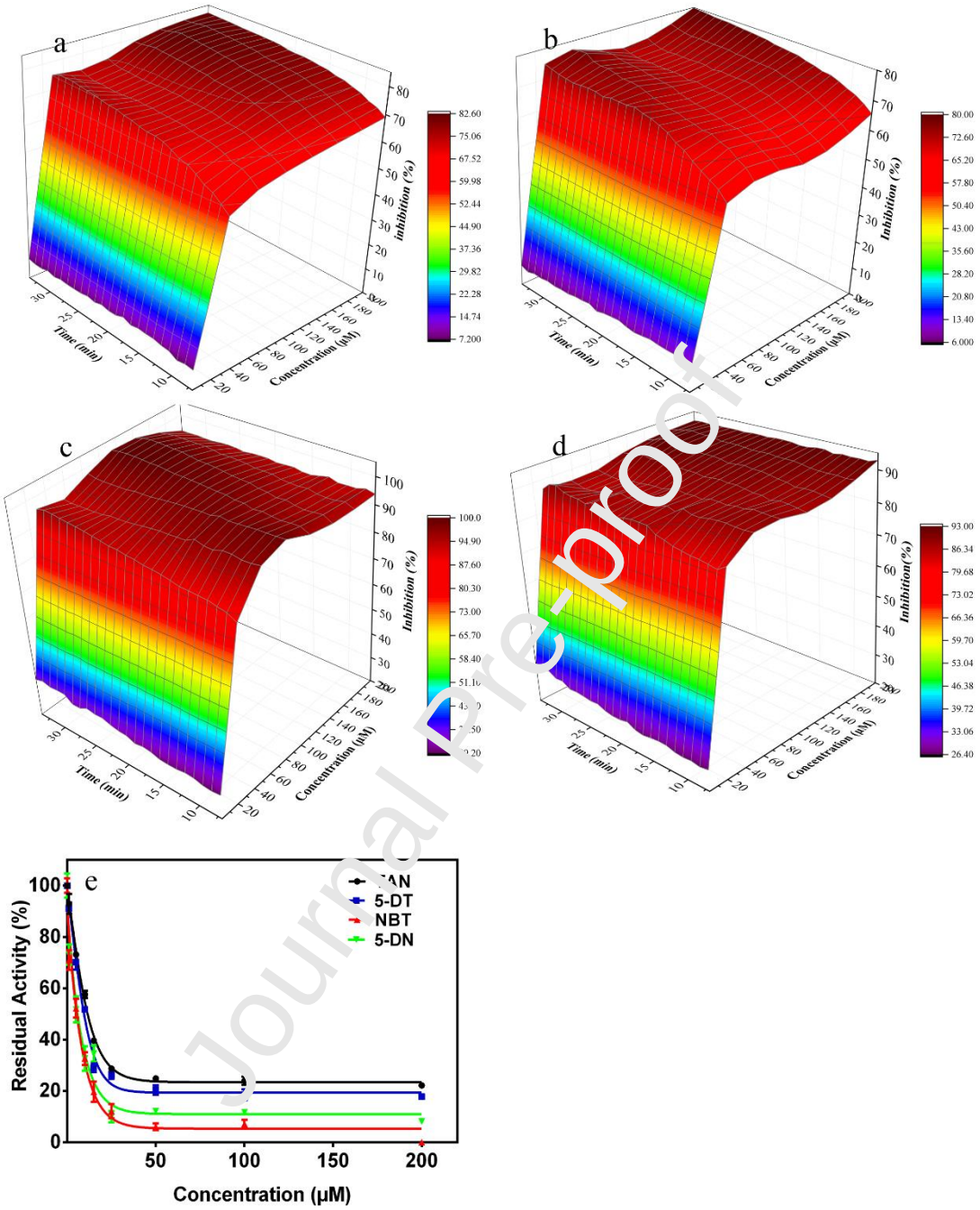

Fig. 4

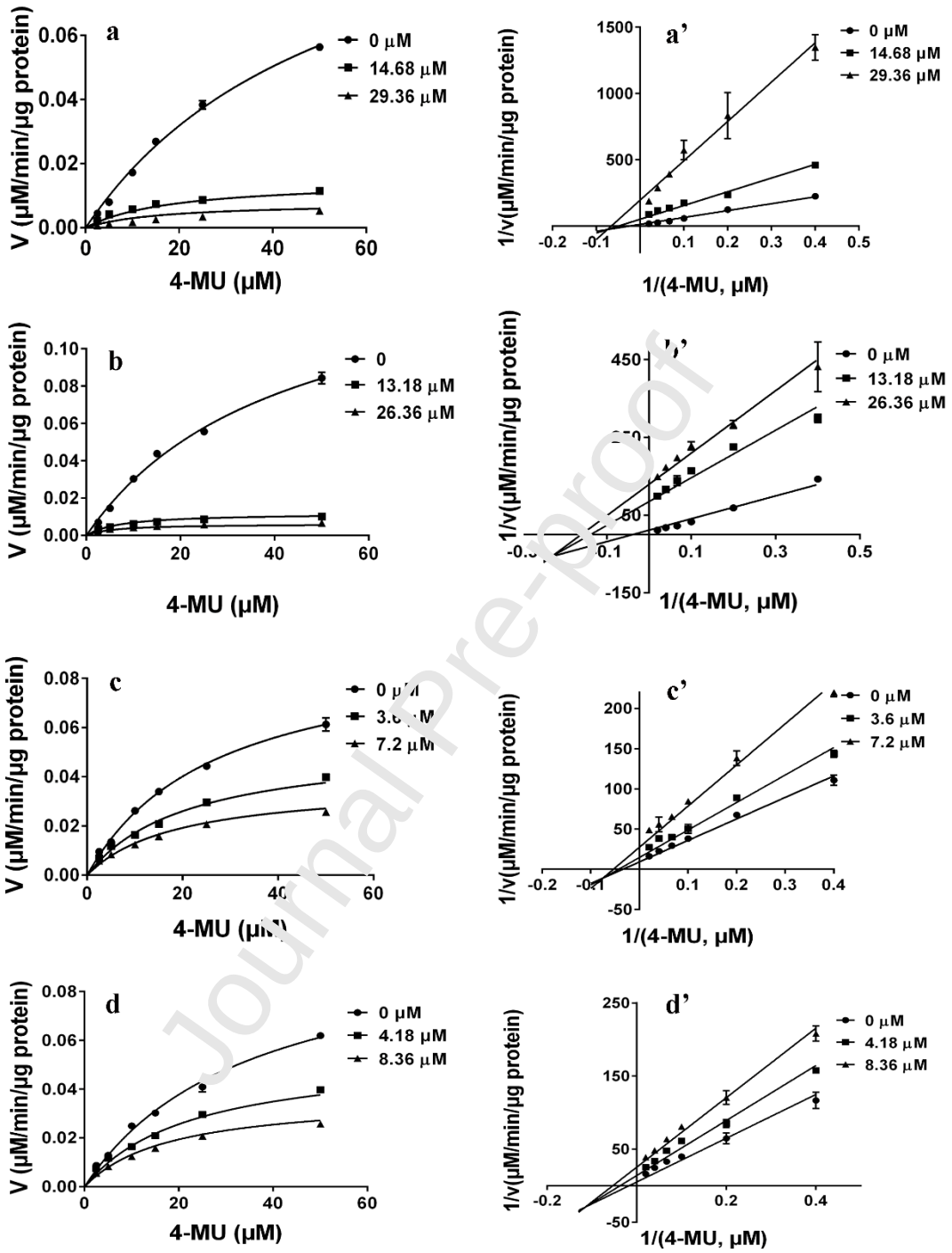

Fig. 5

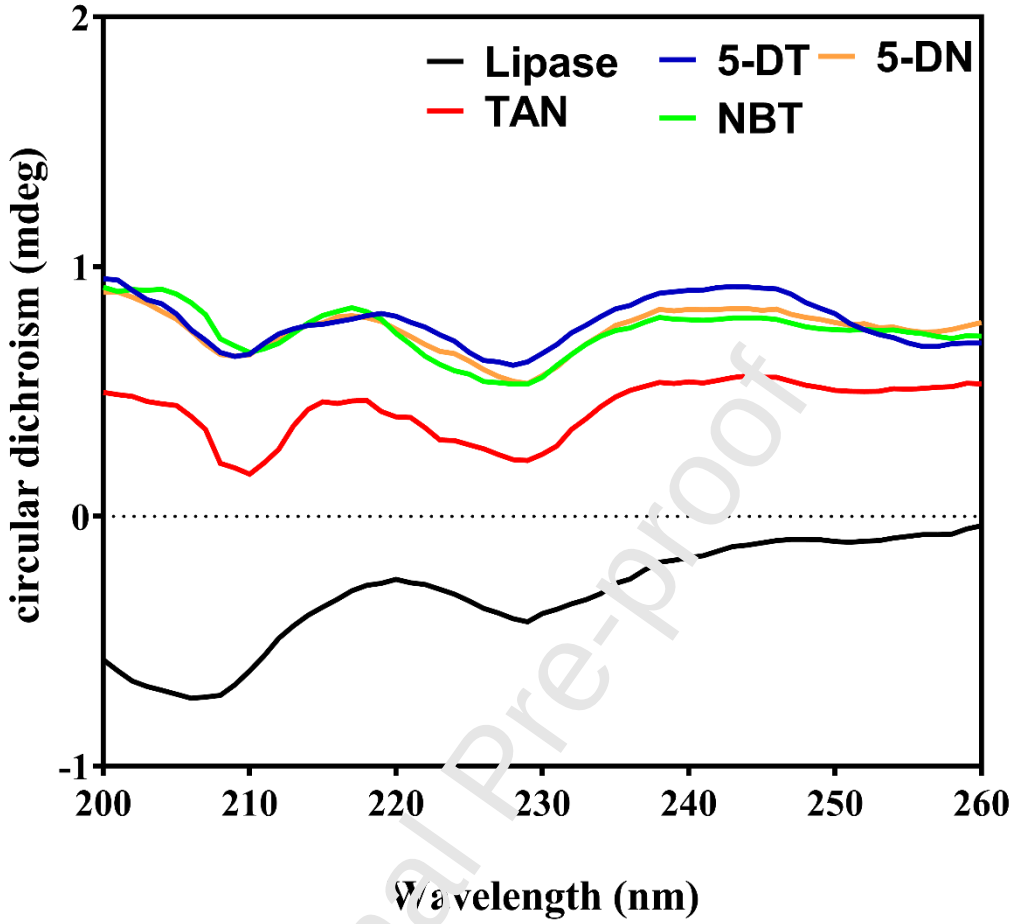

Fig. 6

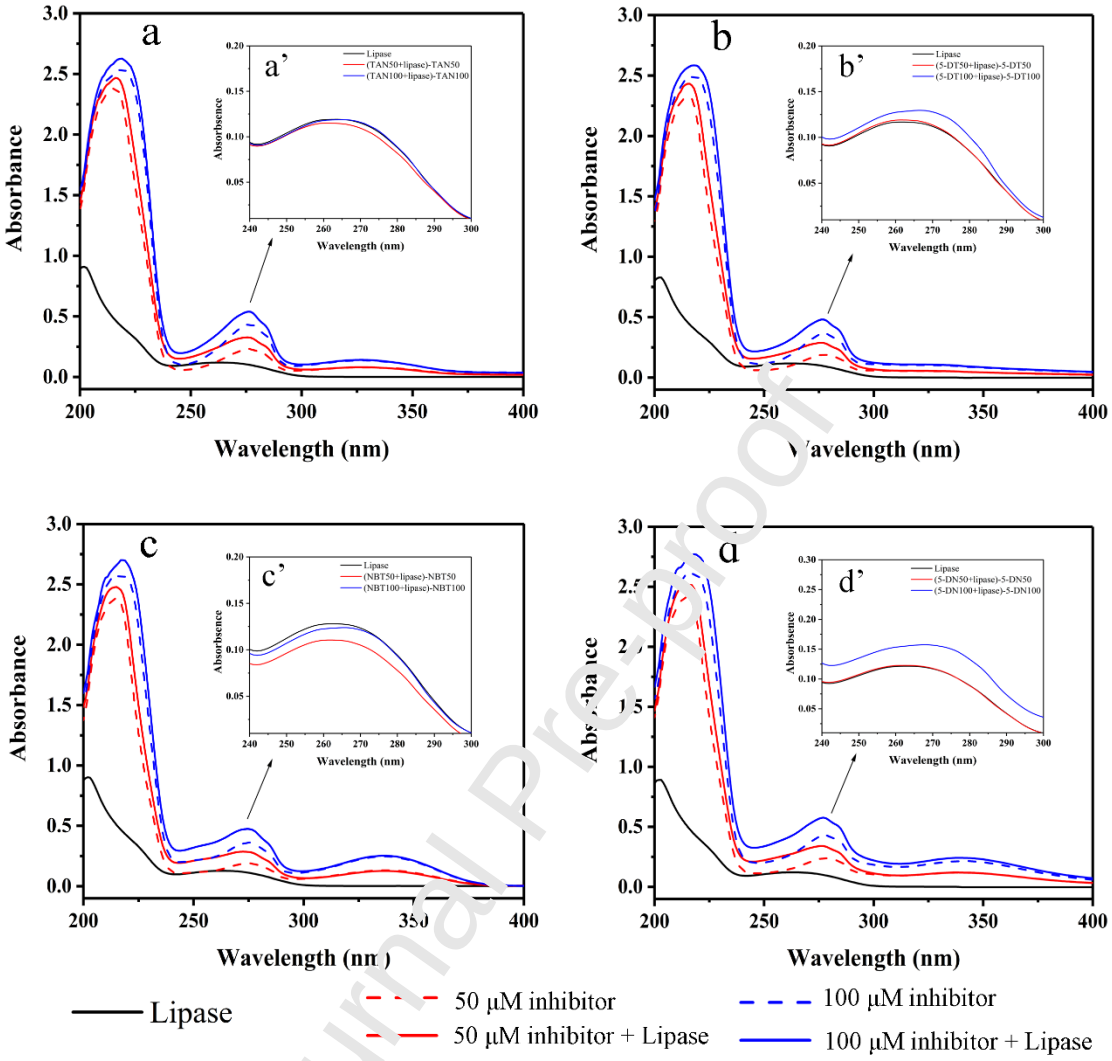

Fig. 7

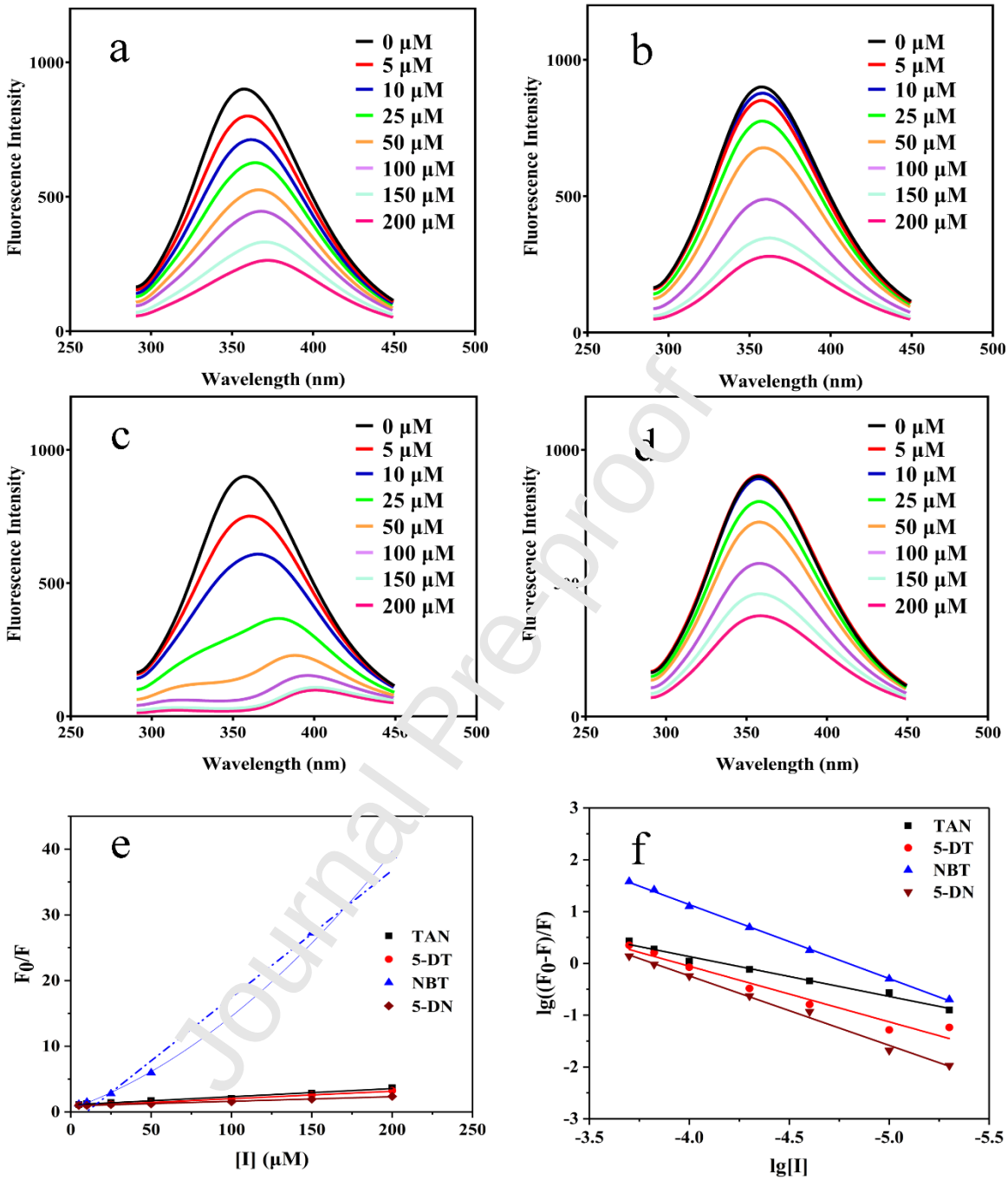

Fig. 8

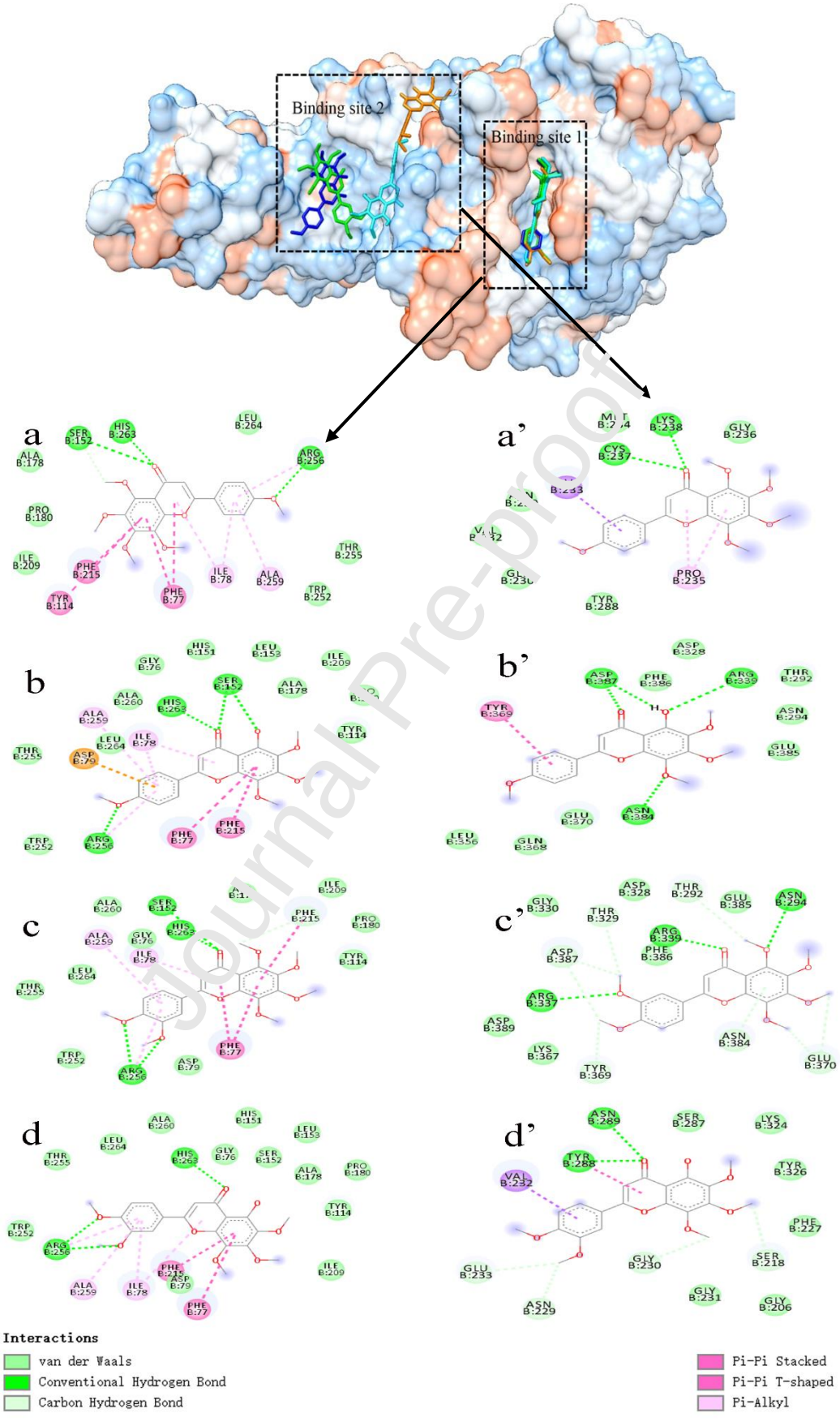

Fig. 9

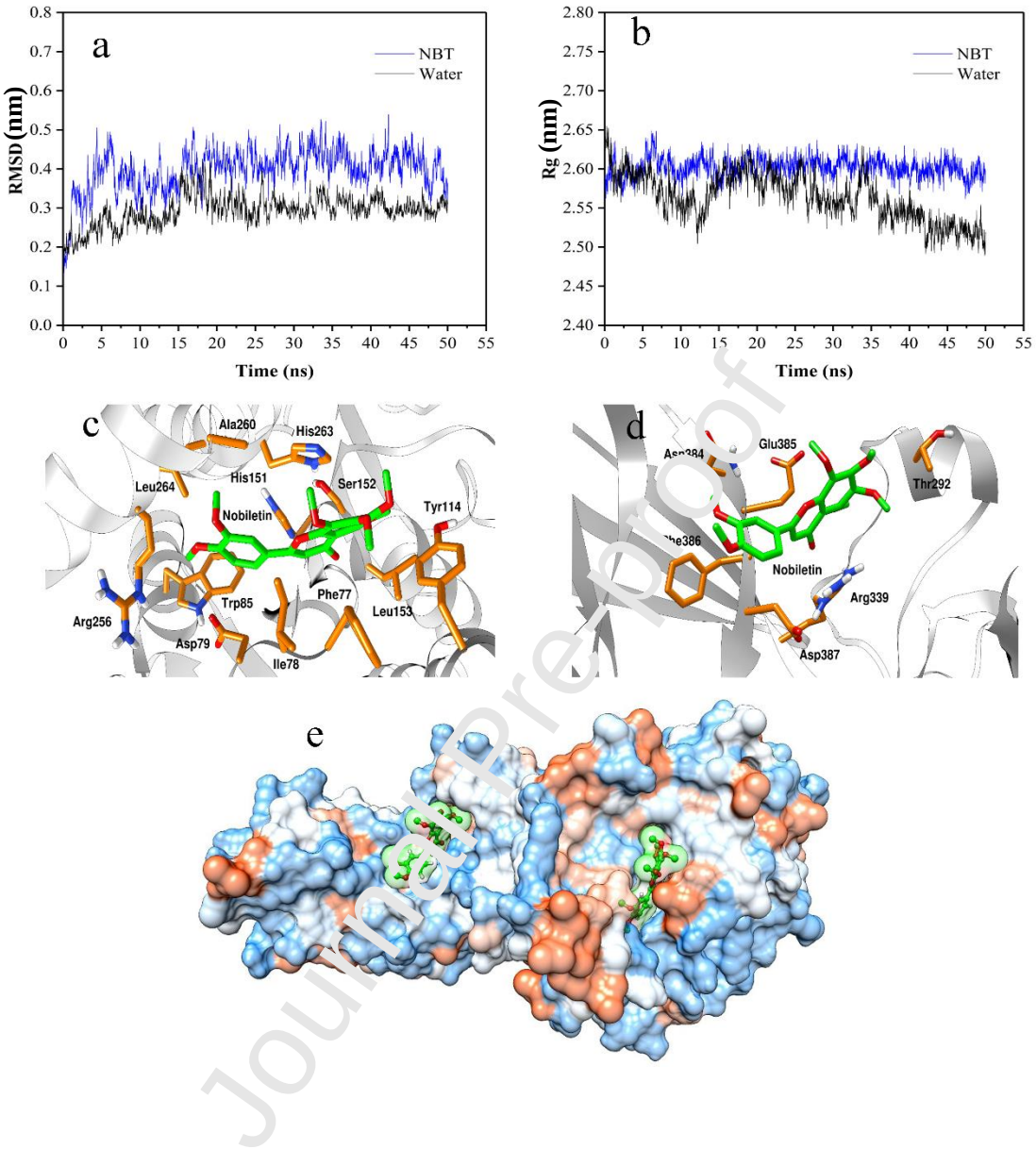

Highlights

- NBT was the strongest lipase inhibitory activity (IC_{50}=3.60±0.19 μM) than other 3 PMFs.
- MD was applied to study the structure-activity relationship of PMFs on PPL.
- The mechanism of PPL inhibition by PMFs was analyzed in vitro and in silico.
- The inhibition of PMF on PPL is related to the -OCH_3 of its 3'-position.